Universal finite-size scaling function for kinetics of phase separation in mixtures with varying number of components

Suman Majumder,[1,*] Subir K. Das,[2,†] and Wolfhard Janke[1,‡]

[1]*Institut für Theoretische Physik, Universität Leipzig, Postfach 100 920, D-04009 Leipzig, Germany*

[2]*Theoretical Sciences Unit, Jawaharlal Nehru Centre for Advanced Scientific Research, Jakkur P.O., Bangalore 560064, India*

(Received 27 July 2018; published 25 October 2018)

From Kawasaki-exchange Monte Carlo simulations of the q-state Potts model, we present results for the kinetics of phase separation in multicomponent mixtures, for $q \leqslant 10$, in space dimension $d = 2$. A particular focus has been on the quantification of finite-size scaling functions for various values of q and quench depths. For a range of final quench temperatures, our analyses, via finite-size scaling and other state-of-the-art methods, show that the growth follows the Lifshitz-Slyozov behavior, expected for a diffusive mechanism, irrespective of the number of components. We show that the growth for different q values and quench temperatures, in finite systems, can be described by a universal scaling function with a nonuniversal metric factor, originating from the differences in the amplitudes. We also demonstrate the morphological and kinetic equivalence between a q-component equal proportion mixture and an off-critical binary mixture, in the framework of the Ising model, with relative concentration of the minority component in the latter being $x_c = 1/q$.

DOI: 10.1103/PhysRevE.98.042142

I. INTRODUCTION

Phase separation in mixtures, following quenches from the homogeneous phase into a region inside the miscibility gap, occurs via the formation and subsequent growth [1–3] of domains, rich in like species. This domain coarsening is typically a scaling phenomenon [1–3], characterized via the collapse of various morphology-describing functions with time t. For example, in standard situations, the two-point equal-time correlation function $C(r, t)$, its Fourier transform, the structure factor $S(k, t)$, and the probability distribution function $P(\ell_d, t)$ of domain lengths ℓ_d exhibit the scaling properties

$$C(r, t) = \tilde{C}[r/\ell(t)], \tag{1}$$

$$S(k, t) = \ell(t)^d \tilde{S}[k\ell(t)], \tag{2}$$

and

$$P(\ell_d, t) = \ell(t)^{-1} \tilde{P}[\ell_d/\ell(t)], \tag{3}$$

respectively, with $\tilde{C}$, $\tilde{S}$, and $\tilde{P}$ being the corresponding time-independent master functions [2]. Here, $\ell(t)$, the average domain length $\overline{\ell}_d$ at time t, is expected to exhibit a power-law growth, at least in the long-time limit, as [2]

$$\ell(t) = At^{\alpha}, \tag{4}$$

with an exponent α and amplitude A. Usually, α is a constant for a particular mechanism, though A depends on quench temperature and other physical conditions. Focus of a large number of studies on phase separation [4–15], where the total value of the relevant order parameter does not change with time, has been on solid binary mixtures, with the objective of estimation of α, via Monte Carlo (MC) simulations [16] of the Ising model. In this case, growth occurs via diffusive transport of material, for which the rate of change of $\ell(t)$ can be written as [2,6]

$$\frac{d\ell(t)}{dt} \sim |\vec{\nabla}\mu| \sim \frac{\gamma}{\ell(t)^2}, \tag{5}$$

where μ and γ are the chemical potential and the interfacial tension, respectively. Equation (5) yields $\alpha = \frac{1}{3}$, known as the Lifshitz-Slyozov (LS) growth exponent [17]. Kinetics of phase transitions in fluids, is, of course, more complex. There, the late time growth is faster due to the influence of hydrodynamics [18–24], and there exist multiple scaling regimes characterized by different values of α, that may again depend upon the morphological features [25–29]. Nevertheless, even in fluids the early time growth is described by the LS exponent [24].

As stated above, the Ising model has been extensively studied [4–15], via MC simulations, to understand the phase separation kinetics in solid binary mixtures. Earlier simulation studies, however, reported values of α which are much smaller than the LS one. Later, it was proposed [6] that $\alpha = \frac{1}{3}$ will only be realized when $\ell(t) \to \infty$ and corrections to the growth law, that may arise from curvature of the domain boundaries at early time, can be taken care of by incorporating higher order terms in Eq. (5), such that

$$\frac{d\ell(t)}{dt} = \frac{C_1}{\ell(t)^2} + \frac{C_2}{\ell(t)^3} + O[\ell(t)^{-4}]. \tag{6}$$

However, in Refs. [9,13,14,30] it has been shown that consideration of an initial domain length ℓ_0 and, thus, quantification

*suman.majumder@itp.uni-leipzig.de
†das@jncasr.ac.in
‡wolfhard.janke@itp.uni-leipzig.de

of the growth as

$$\ell(t) = \ell_0 + At^{\alpha}, \tag{7}$$

could possibly be a simple explanation of such "effective" finite-time correction to the scaling. The length ℓ_0 can be considered to be analogous to the background contribution that has been often used in the analysis of data in critical phenomena (see references in Ref. [31]). It was demonstrated that an appropriate finite-size scaling analysis can estimate the value of ℓ_0 accurately and, thus, help identification of the LS exponent from much earlier times [13,14].

The above discussion is primarily related to binary mixtures. Although one expects a similar picture for a multicomponent mixture (with the number of components $q > 2$), there exist much fewer simulation studies [5,32–35] for the latter case. Such a q-component mixture could be well understood via the q-state Potts model [36] having the Hamiltonian

$$H = -J \sum_{\langle ij \rangle} \delta_{\sigma_i,\sigma_j}; \quad \sigma_i = 1, 2, \ldots, q; \; J > 0 \tag{8}$$

where $\langle ij \rangle$ indicates summation over nearest neighbors. In the thermodynamic limit, the critical temperature for this model [36] is $T_c = J/[k_B \ln(1 + \sqrt{q})]$, where k_B is the Boltzmann constant. For $q \leqslant 4$ the model exhibits second-order phase transitions, while for $q \geqslant 5$ the transitions are of first-order type [36]. For $q = 2$, this model Hamiltonian corresponds, of course, to that of a binary mixture that differs from the Ising model Hamiltonian by a factor of 2. In the case of Potts model also earlier MC simulations [5] with $q \leqslant 6$ yielded a much smaller exponent, viz., $\alpha \simeq 0.2$. Later, it was shown that the LS growth is recovered in the asymptotic limit [32], like in the Ising case. This was further confirmed [35] via a renormalization-group method of analysis [7,8] of MC simulation results for $q \leqslant 10$.

The application of finite-size scaling analysis, along with the consideration of ℓ_0 [see Eq. (7)], provided the realization that the correction to the LS growth law is rather weak, at least for the Ising model [13,14]. Recently, such analysis has also been applied successfully to understand the cluster coarsening during the collapse of a polymer [37–39]. In this context, it has been shown that such cluster growth at different quench temperatures T (or solvent conditions) can be described by a universal finite-size scaling function with a nonuniversal metric factor, related to the amplitudes of growth [38,39]. A primary requirement for the universal nature of the finite-size scaling function is that the corresponding effects must emerge at the same value of the ratio between the characteristic length scale and its equilibrium limit. An affirmative answer with respect to this was provided [15] in an earlier work on the Ising model with different mixture compositions. Inspired by these works, we revisit the q-state Potts model in space dimension $d = 2$, and search for the existence of a universal finite-size scaling function for different q and quench temperature. This is by considering the status that an equivalence between the Ising and the Potts model, for conserved order-parameter dynamics, has not yet been established and is not obvious, although it has already been proposed in the context of nonconserved order-parameter dynamics [40,41]. Furthermore, even if the onset of finite-size effects occurs at the same value of the above mentioned ratio, the forms of the corresponding full scaling functions need not be the same. To this end, we also present more comprehensive results from the Ising model, with varying compositions, and aim to establish a kinetic equivalence of it with the Potts model.

The rest of the paper is organized as follows. Section II describes the details of simulations and methods of calculation of necessary observables, along with a brief description of the formulation of finite-size scaling analysis. The results are presented in Sec. III. Finally, we conclude the paper in Sec. IV with a brief summary and outlook.

II. METHODS

A. Simulation details and calculation of observables

Given that the Ising model is a special case of the Potts model, we describe the methods with reference to the Potts model only. We perform MC simulations [16] on square lattices having linear dimension La in each Cartesian direction, where a is the lattice constant, which we set to unity. We apply periodic boundary conditions in both the directions. Dynamics is introduced via the standard Kawasaki exchange mechanism [16,42] that conserves the order parameter, i.e., the overall concentration of each state remains fixed during the entire evolution. In this method, a typical MC move consists of interchange of positions between a randomly chosen pair of nearest-neighbor spins σ_i. The move is accepted or rejected according to the standard Metropolis algorithm that compares a random number with the associated Boltzmann factor [16]. A total of L^2 such attempted exchanges form a MC step (MCS), the unit of time in our simulations.

Random mixtures of all the spin states in equal proportion are prepared as initial configurations, which mimic the high-temperature ($T = \infty$) homogeneous phase. Such configurations are then suddenly quenched to a temperature below T_c. In our simulations, J/k_B is the unit of temperature, and for convenience both J and k_B are set to unity. For finite lattices of size L, when the transitions are of second-order type, the finite-size critical temperatures T_c^L scale with the system size as $|T_c^L - T_c| \sim L^{-1/\nu}$, where ν is the critical exponent corresponding to the equilibrium correlation length. For a first-order transition, $L^{-1/\nu}$ is replaced by L^{-2} (the inverse volume in two dimensions). Given that our lattice sizes are sufficiently large, we do not expect the values of T_c^L to differ significantly from the thermodynamic values, irrespective of a first- or a second-order transition. In fact, data from various models suggest that for the considered lattice sizes values of T_c^L will differ from the thermodynamic value by less than a percent [43].

We consider three different system sizes with $L = 64$, 128, and 256, and the respective presented data sets (except for the evolution snapshots) are averaged over 150, 100, and 50 different initial realizations. In the case of the Ising model, we have performed simulations for different compositions by fixing the area fraction of the minority species in such a way that it matches to that of one of the components for the $q > 2$ Potts model.

The prime quantity of interest in this work is the average linear size of the domains. It can be calculated by using the

scaling properties of morphology characterizing functions [2]: (i) from the decay, e.g., the first-zero crossing, of the two-point equal-time correlation function

$$C(r,t) = \frac{1}{q}\sum_{n=1}^{q}\left[\left\langle \psi_i^n(t)\psi_j^n(t)\right\rangle - \left\langle \psi_i^n(t)\right\rangle\left\langle \psi_j^n(t)\right\rangle\right], \quad (9)$$

where r is the scalar distance between sites i and j, $\psi_i^n = 2\delta_{\sigma_{i,n}} - 1$ and $\langle \dots \rangle$ denotes statistical averaging; (ii) via the calculation of the first moment of $S(k,t)$; and (iii) from the first moment of the normalized domain-length distribution function $P(\ell_d, t)$ as

$$\ell(t) = \overline{\ell}_d = \int d\ell_d \; \ell_d P(\ell_d, t), \quad (10)$$

where the length ℓ_d is the separation between two successive interfaces in the x or y direction. The variable ψ_i^n has been defined in such a way that it takes the values ± 1, like the Ising spin variable. In addition to convenience, this transformation, thus, will also facilitate comparison between the two models. The transformation of σ_i to ψ_i^n essentially implies that to any of the q states, the rest of the $(q-1)$ states are equivalent [35], in line with the definition of the Potts Hamiltonian. All the above methods provide measures of $\ell(t)$ proportional to each other [14]. In this work we will use $\ell(t)$ obtained from method (i) for demonstrating the scaling of $C(r,t)$ and $S(k,t)$, whereas for the rest of the purposes we will use $\ell(t)$ from Eq. (10).

Having mentioned the various ways of estimating $\ell(t)$, it should be kept in mind that the presence of noise clusters of the size of $\xi(T)$ (where ξ is the equilibrium correlation length) often prevents the accurate estimation of the domain sizes, particularly at higher temperatures. To avoid such unwanted features, we analyze noise-free snapshots by eliminating clusters of the size of ξ via a majority spin rule. In this method, the spin value at a site i is replaced by the sign of the majority of the spins sitting at i and nearest neighbors of i. Note that depending on the temperature, the sizes of the noise clusters vary. Hence, the method of elimination also changes either by performing several iterations of the above process or by considering more distant neighbors. For a clear picture of how this noise removal works, we refer to the case of the Ising model in Ref. [14].

B. Finite-size scaling

Introduced in the context of equilibrium critical phenomena [44–46], the finite-size scaling (FSS) technique finds it application in diverse variety of problems involving diverging length scales. Since the FSS method will be used extensively to analyze data in this work, here, in brief, we discuss the basic concepts of the method. First, we introduce it in the context of equilibrium critical phenomena [16,44–46], in analogy with which we will discuss the nonequilibrium case [11–14,30].

In the thermodynamic limit ($L \to \infty$), the singularity of a quantity X, thermodynamic or dynamic, in the vicinity of the critical temperature T_c, is quantified as

$$X = X_0|T - T_c|^{-x}, \quad (11)$$

where x is the corresponding critical exponent, X_0 being the amplitude. For instance, the central quantity, the correlation length ξ, diverges with an exponent ν as

$$\xi = \xi_0|T - T_c|^{-\nu}. \quad (12)$$

Using Eq. (12) in Eq. (11) one gets

$$X = \tilde{X}_0 \xi^{x/\nu}, \quad (13)$$

with $\tilde{X}_0 = X_0 \xi_0^{-x/\nu}$. In computer simulations, building of correlations at criticality is restricted by the size of the system and thus $\xi \sim L$. Substitution of this fact in Eq. (13) provides

$$X = \tilde{X}_0 L^{x/\nu}. \quad (14)$$

Far away from the critical point, for $\xi \ll L$, this restriction does not apply. To bridge such finite-size limit behavior with that of Eq. (13), one introduces a scaling function $Y(y)$, independent of system size, to write

$$X = Y(y) L^{x/\nu}, \quad (15)$$

where the scaling variable y is dimensionless, a natural choice for which is L/ξ or some power of it. While for static quantities the behavior of $Y(y)$ has been addressed (see references in Ref. [31]), the corresponding knowledge is limited for dynamics. Nevertheless, one can deduce the limiting behavior. For $\xi/L \gg 1$ (ξ having the value expected in the thermodynamic limit),

$$Y(y) = \tilde{X}_0, \quad (16)$$

since arriving at Eq. (14) is a necessity. In the other limit, where $\xi/L \ll 1$, for the choice $y = (L/\xi)^{1/\nu}$, one must have

$$Y(y) \sim y^{-x}, \quad (17)$$

such that Eq. (13) [or Eq. (11)] is recovered. By tuning the value of the exponent x one looks for optimum collapse of data obtained from simulations of finite systems of different sizes, behavior of which should be consistent with Eqs. (16) and (17). This allows one to extract the exponent x.

Having provided a general discussion on FSS analysis in the context of critical phenomena, we turn our attention to the nonequilibrium domain-growth problem which is of our interest here. As in Refs. [13,14,30], here also we intend to quantify the growth of the average domain length as

$$\ell(t) = \ell_0 + A(t - t_0)^{\alpha}, \quad (18)$$

where ℓ_0 could be interpreted as the average characteristic length when the system becomes unstable to fluctuations, after a time t_0 from the instant of quench. On expanding Eq. (18) for $t \gg t_0$ one gets

$$\ell(t) = \ell_0 + At^{\alpha} - At_0\alpha t^{\alpha-1} + \cdots. \quad (19)$$

For LS growth ($\alpha = \frac{1}{3}$) this implies that the contribution of t_0 is insignificant compared to ℓ_0, and thus Eq. (18) reduces to Eq. (7). In the thermodynamic limit even the subtraction of ℓ_0 does not make a significant difference in the estimation of the growth exponent α. However, for finite systems, that can be simulated in computers, it does. We construct the FSS formalism by using the analogy $\ell(t) - \ell_0 \hat{=} \xi$ and $1/(t - t_0) \hat{=} |T - T_c|$. Like in critical phenomena, as discussed above, here also we account for the finite-size effects by invoking the scaling function $Y(y)$ such that $\ell(t) - \ell_0 = (\ell_{\max} - \ell_0)Y(y)$,

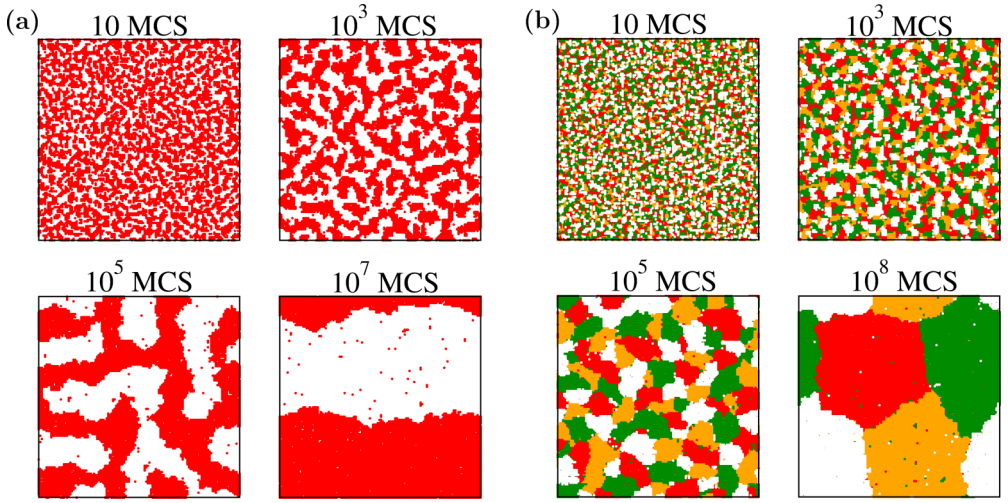

FIG. 1. Evolution snapshots at different times for (a) $q = 2$ and (b) $q = 4$. These pictures were obtained from the MC simulations of the q-state Potts model, following quenches from the high-temperature homogeneous phase to $T = 0.7\,T_c$, that lies inside the miscibility gap. For both values of q, the used system size is $L = 128$. Different colors (gray shades) correspond to different states.

which implies

$$Y(y) = \frac{\ell(t) - \ell_0}{\ell_{\max} - \ell_0}. \tag{20}$$

Notice that we have replaced L by $\ell_{\max}$ ($\sim L$), the saturation or the equilibrium domain length a finite system can attain. In the next section, we will show how we estimate it. Now, for the choice [30] of the dimensionless scaling variable

$$y = \frac{(\ell_{\max} - \ell_0)^{1/\alpha}}{(t - t_0)}, \tag{21}$$

in the early time regime one must have

$$Y(y) \sim y^{-\alpha}, \tag{22}$$

so that Eq. (18) is recovered. On the other hand, in the finite-size limit ($y \to 0$) one gets $Y(y) \to 1$. In the FSS exercise our objective will be to obtain an optimum collapse of data, coming from simulations of different finite system sizes, along with the satisfaction of the above two limiting forms of $Y(y)$. For this purpose, one can use both ℓ_0 (or t_0) and α as adjustable parameters. However, we will estimate ℓ_0 (or t_0) from a separate reliable analysis, so that the FSS analysis becomes more trustworthy.

III. RESULTS

A. Morphological features

Figure 1 shows typical evolution morphologies, obtained from our MC simulations of the Potts model, for (a) $q = 2$ and (b) $q = 4$, at $T = 0.7\,T_c$. The $q = 2$ case, showing presence of interconnected percolating structures, essentially represents the Ising model scenario with 50:50 composition. For higher q value, the evolving pattern consists of disconnected domains. This resembles the dropletlike morphology [15] that one observes during evolution in off-critical binary mixtures, as in the Ising model with fixed nonzero overall magnetization. It has to be noted that the growth of domains occurs via reduction of the interface area. For high values of q, the presence of the point defects, i.e., meeting points of three or more different states (colors in the figures), will be high, particularly at early time. What role such defects will play during the coarsening process in the Potts model is unclear. Physically, point defects in the Potts model are different from those in the clock model [36], which in the $q \to \infty$ limit corresponds to the dynamical XY model [2]. Growth in the latter case occurs via annihilation of these topological point defects with opposite charges [2], decided by the sign of the phase change (in integral multiples of 2π) along a closed loop around the point under consideration. In the present case, given that the energy penalty at the interface between any two dissimilar phases is the same, unlike in the clock model, we do not expect any particular order for the appearance of different states around a point defect and, thus, the definition of the topological charge in this problem may not be meaningful. In any case, since we consider $q \leqslant 10$, even at moderately late time the growth essentially occurs via the annihilation of (one-dimensional) interfaces. Notice that the snapshots in Fig. 1 contain significant impurities or noise within the domains. This feature, prominent at high temperature, does not allow one to calculate the domain sizes accurately [13,14]. As already mentioned in Sec. II A, for all the subsequent analyses we remove such noise to work with pure-domain morphology.

In Fig. 2 we demonstrate the scaling properties of the structure during the ordering process for $q = 4$, by plotting various morphology characterizing functions, in accordance with the expectations in Eqs. (1)–(3). In the log-log plot of Fig. 2(b), the solid line corresponds to the Porod tail ($\sim k^{-3}$) [47], arising due to the short distance ($r \ll \ell$) singularity [2,3] in $C(r, t)$, that captures the scattering from sharp interfaces. For the other limit, i.e., when $k \to 0$, $S(k, t)$ is expected to follow the Yeung's law ($\sim k^4$) [48], understood to be a consequence of the order-parameter conservation [3]. Our data, however, are consistent with a k^2 behavior, represented by the dashed line. Such a weak enhancement is consistent with the study of kinetics in binary mixtures with off-critical composition, for which one observes dropletlike domains. Even a weaker dependence, viz., $S(k \to 0) \sim k^{0.9}$, has been

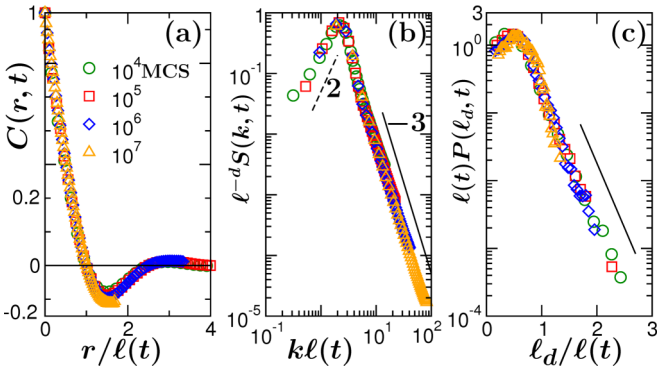

FIG. 2. Demonstration of the scaling of (a) the correlation function $C(r,t)$, (b) the structure factor $S(k,t)$, and (c) the domain-length distribution function $P(\ell_d,t)$, for $q=4$, at $T=0.7\,T_c$, with $L=128$. The solid and the dashed lines in (b) correspond to k^{-3} (Porod law) and k^2 behavior, respectively, whereas the solid line in (c) represents an exponential decay.

recently observed during coarsening in a ballistic aggregation model, where domains have "perfectly" circular-droplet morphology [49]. In Fig. 2(c), the tail of the data shows a linear behavior on a semi-log plot, indicating an exponential decay [33–35] of $P(\ell_d,t)$.

To obtain a quantitative information on the differences in morphologies for different q, in Fig. 3 we plot the scaled functions (a) $C(r,t)$, (b) $S(k,t)$, and (c) $P(\ell_d,t)$, at $t=10^5$ MCS, for a few values of q. Clearly, nonunique features are visible. For $C(r,t)$ one can notice a monotonic decrease in the depth of minimum with the increase of q. This resembles the scenario during evolution of the Ising model with different compositions of up and down spins. While this fact was separately demonstrated for the Potts [35] and the Ising [15] models, a direct comparison between the two cases will be interesting. Other important features in Fig. 3 are related to the decrease of the power-law exponent for the small k behavior of $S(k,t)$, from $\simeq 4$ to smaller values, with the increase of q and faster decay of $P(\ell_d,t)$, for similar variation of q. Next, we proceed to present a comparative picture between the Ising and the Potts models.

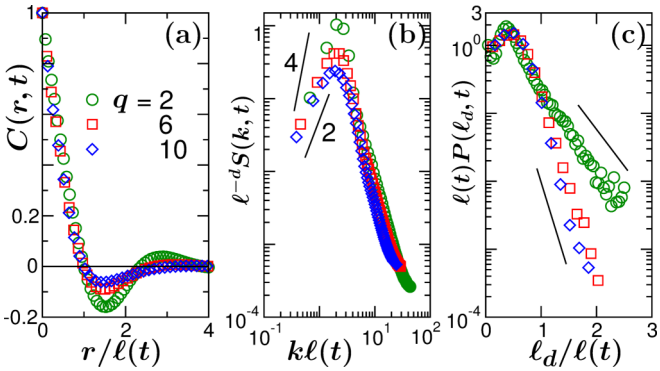

FIG. 3. Plots comparing the scaled (a) correlation function $C(r,t)$, (b) structure factor $S(k,t)$, and (c) domain-length distribution function $P(\ell_d,t)$, for different q. For all values of q, the results correspond to $L=128$, $T=0.7\,T_c$, and $t=10^5$ MCS.

As already stated, for the Ising model, instead of using equal proportion of the two components, we use asymmetric compositions. Since our goal is to compare a q-component mixture with a binary mixture having $x_c=1/q$, we simulate two systems in parallel: the q-state Potts model and the two-state Potts model where the minority component has $x_c=1/q$, given that the Potts model with $q=2$ is equivalent to the Ising model, as previously noted, apart from a factor of 2 in the Hamiltonian. (Nevertheless, for the sake of convenience of presentation, the studies of the two-state Potts model related to the composition dependence in binary mixture will be referred to as coming from the Ising model.) We have performed this comparative study for different values of q. In all these simulations, we fix the quench temperature to $0.6J/k_B$, instead of setting it to a fixed fraction of the ratio T/T_c, to have a comparable strength of noise. Note that, in general, the strength of noise depends on how far T is from the critical point since the size of the noise clusters directly correspond to the equilibrium correlation length. However, there exists ambiguity with respect to the amplitude of critical singularity of correlation length as well as with respect to the order of transition when one varies q in the Potts model. We have checked that the above choice provides a more comparable noise in the two cases than that for simulations at a fixed ratio of T/T_c.

In Fig. 4 we show snapshots of q-component mixtures and the corresponding binary mixtures, for two different values of q. For both the values of q, there exists a strong similarity between the Potts and the Ising model snapshots, with respect to the pattern as well as growth, even though there is some degree of dissimilarity concerning the strength of noise, particularly for large value of q (at early time). In any case it can be appreciated that the patterns appear to be consisting of nearly circular droplets, at late time, in both the cases.

Figure 5 shows comparison of various morphology-characterizing functions for the systems in Fig. 4. For both values of q, the scaled correlation functions and the structure factors from the Ising and the Potts models overlap with each other reasonably well. On the other hand, in the tail regions of the scaled domain-length distribution (which is very sensitive to noise) there exist differences, noticeable particularly for the $q=10$ case. Although we calculate all these functions from noise-removed morphologies, this difference could be attributed to differences in the size of the noise clusters between the two models at the concerned temperature. One can argue that this could be tackled by performing several iterations or considering farther neighbors during the noise-removal exercise. However, for large q such exercise could destroy the original morphology, given that with the increase of q, at a particular time, the value of ℓ decreases.

B. Domain growth

Next, we focus on the central objective of this paper, i.e., on understanding of the domain growth kinetics. In Figs. 6(a) and 6(b) we show the plots for the time dependence of $\ell(t)$, for $q=2$ and 6, respectively. All these results were obtained for quenches to $T=0.7\,T_c$. The data for a smaller system size follow those of the larger ones almost until saturation occurs due to the finite-size restriction [13,14]. Estimation of

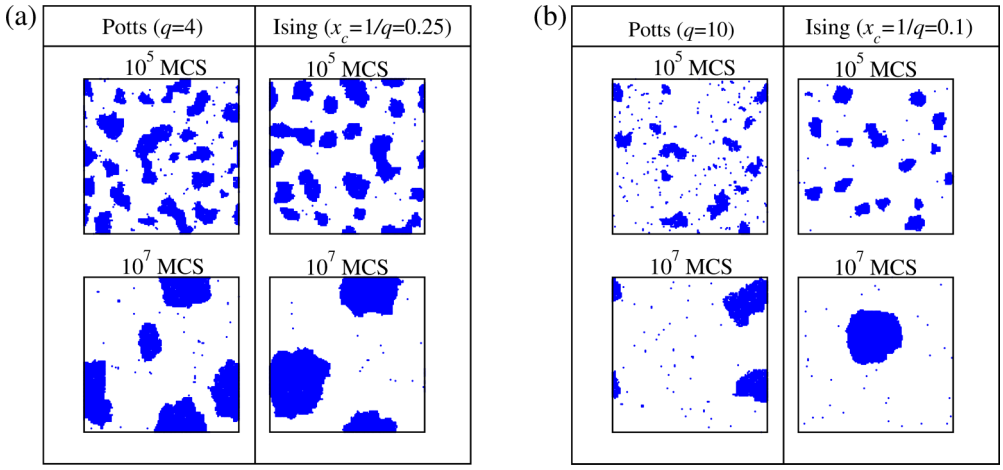

FIG. 4. Comparison of evolution snapshots, at two different times, between equiproportion q-component mixtures and off-critical binary mixtures, concentrations of the minority species (x_c) for the latter being set to $1/q$. Results for two values of q are shown, viz., (a) $q = 4$ and (b) $q = 10$. These results were obtained from simulations at $T = 0.6J/k_B$, using $L = 128$. While for the multicomponent mixtures, positions of particles of one particular component ($\sigma_i = 1$) are shown, for the binary mixture, positions of the minority particles are shown.

this saturation length, for $L = 64$, has been demonstrated in Fig. 6(a). The solid lines in these figures correspond to power-law growth with exponent $\frac{1}{3}$, the LS value. While a smaller system apparently shows a slower growth than the expected LS behavior, one can clearly identify that as the system size increases the data in the long-time limit becomes more and more consistent with the LS growth. This behavior may not be related to (interface) curvature dependent corrections to the scaling; for discussions in connection to the Ising model, see Refs. [13–15]. Here, note that a log-log plot, for the extraction of α, may often be misleading. Because of this reason, calculation of the instantaneous exponent [6]

$$\alpha_i = \frac{d \ln \ell(t)}{d \ln t}, \tag{23}$$

and estimation of α from the convergence of α_i in the $t \to \infty$ limit was prescribed. However, even for such analysis, the data for α_i should be appropriately interpreted [9,13,14]. Typically, when plotted as a function of $1/\ell(t)$, α_i exhibits a linear behavior and only in the limit $\ell(t) \to \infty$ one recovers the LS value $\frac{1}{3}$. While such a linear dependence was previously thought to be due to the correction coming from interfacial curvature, following the arguments presented in Refs. [9,13,14] we will demonstrate later that this behavior can be understood by considering the presence of an initial domain length ℓ_0 [see Eq. (7)], a true physical fact for the Potts model as well.

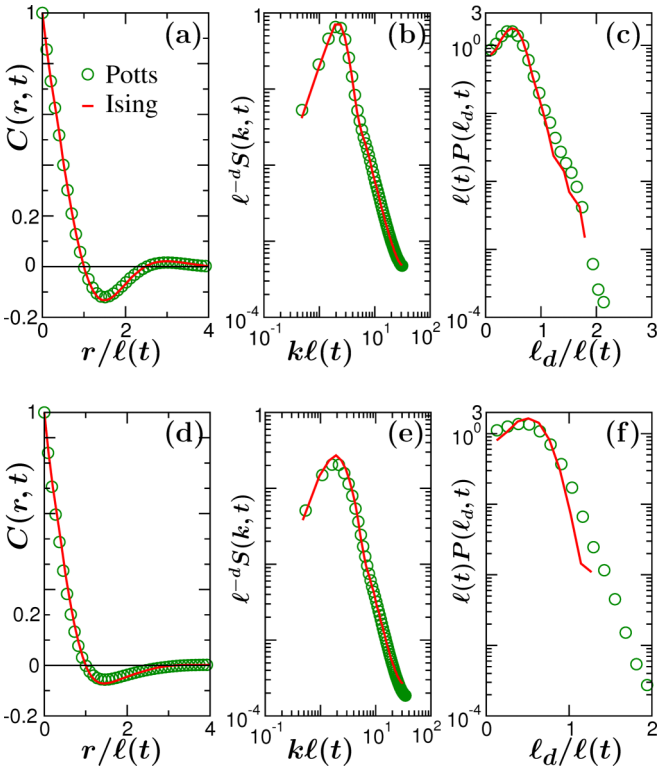

FIG. 5. Plots comparing the scaled correlation function $C(r,t)$, structure factor $S(k,t)$, and domain-length distribution function $P(\ell_d,t)$ for a fixed time ($t = 10^5$ MCS), between the q-state Potts model and the Ising model having concentration of the minority component $x_c = 1/q$. Results in (a), (b), and (c) correspond to $q = 4$ and those in (d), (e), and (f) are for $q = 10$. All data sets correspond to $L = 128$ and $T = 0.6J/k_B$.

Figure 7 shows the comparison in the growth of $\ell(t)$ for different q, at $T = 0.7\,T_c$ with $L = 128$. While on the double-log scale the data apparently look parallel to each other, a careful inspection would reveal the fact that as q becomes larger the slope becomes slightly smaller. However, later it will be clear that this behavior is due to the delayed arrival at the scaling regime for higher q. From this figure, it is evident that the domain length saturates at smaller values for larger q. This is expected if the system size is the same for all q values, as is the case here. For a q-component system of fixed linear dimension L, one expects that the maximum domain length, that can be attained by an individual component, scales with q as

$$\ell_{\max} \sim q^{-1/d}. \tag{24}$$

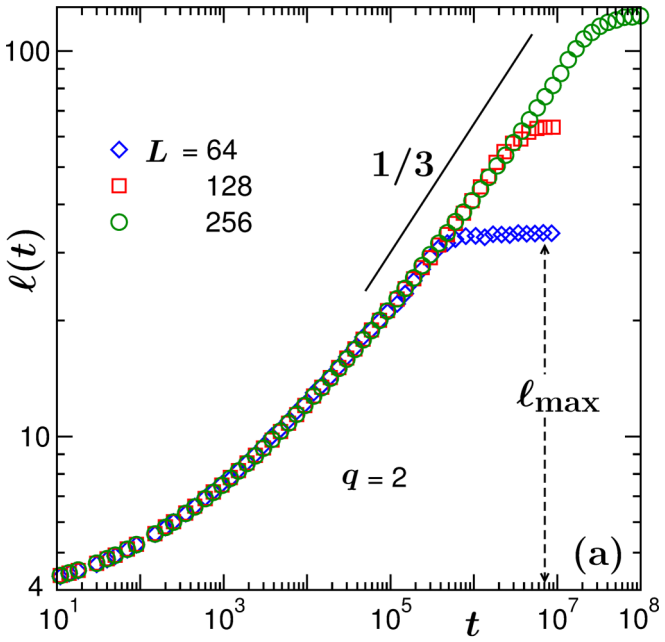

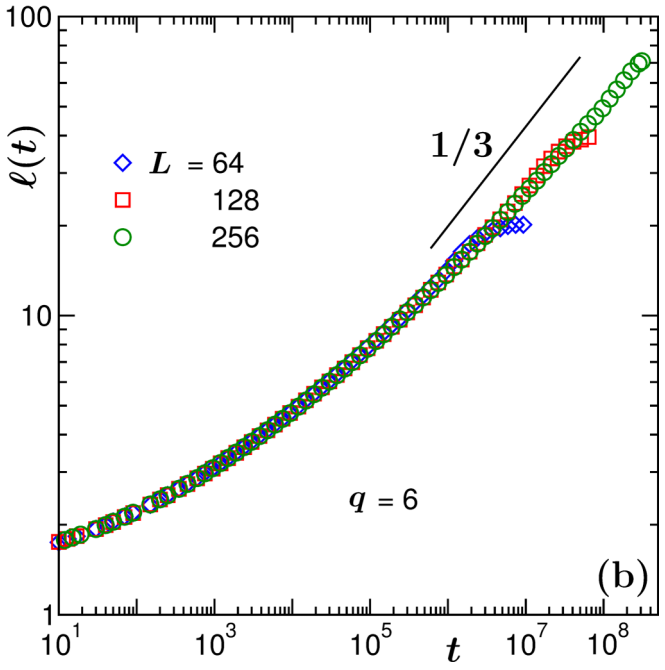

FIG. 6. (a) Double-log plots of the average domain length $\ell(t)$ versus time, for three different system sizes, as indicated, for $q = 2$ at $T = 0.7\,T_c$. (b) Same as (a) but for $q = 6$. The solid lines correspond to the LS growth law. In (a) we also show how we measure the value of the saturation domain length $\ell_{\max}$.

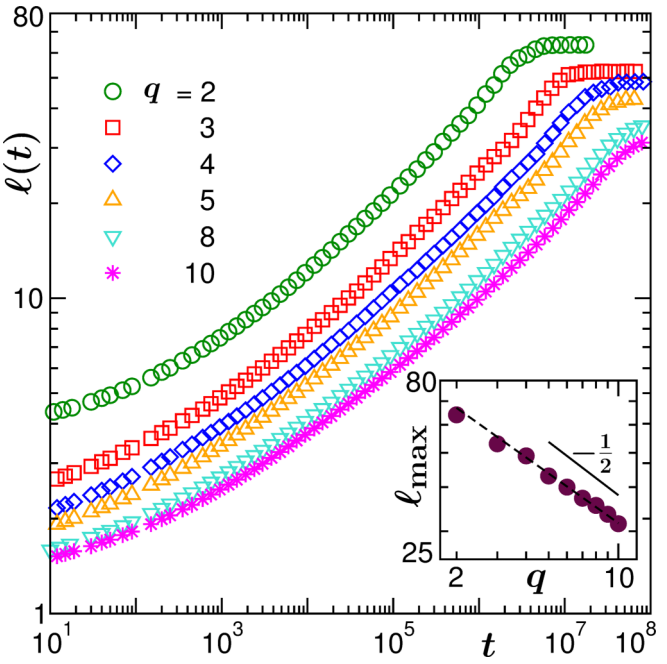

FIG. 7. Double-log plots of the average domain length $\ell(t)$ versus time. Data for few different q-component mixtures are presented, all from $T = 0.7\,T_c$, using $L = 128$. Inset: plot showing the dependence of the saturated domain length $\ell_{\max}$ on q. The dashed line is a fit to the form $\ell_{\max} = Kq^{-\eta}$, that yields $\eta = 0.45$. The solid line shows the expected power-law decay with an exponent $\frac{1}{2}$, corresponding to the behavior noted in Eq. (24).

In the inset of Fig. 7 we show a plot of $\ell_{\max}$ as a function of q, for $L = 128$, obtained at $T = 0.7\,T_c$. The data are found to be fairly consistent with the solid line that represents the behavior quoted in Eq. (24), when d is substituted by 2. A fitting to the form $\ell_{\max} = Kq^{-\eta}$ yields $\eta = 0.45(2)$. Next, we calculate the instantaneous exponent α_i for the data presented in Fig. 7.

The data for α_i, as a function of $1/\ell(t)$, for different q, are shown in Fig. 8. Indeed, one observes reasonable linear behavior. Such extrapolations to $1/\ell(t) \to 0$ yield $\alpha \simeq \frac{1}{3}$, for all q. As pointed out for binary mixtures in Refs. [9,13,14], this linear dependence of α_i could be obtained by using Eq. (7) in Eq. (23). Essentially, one gets

$$\alpha_i = \alpha\left[1 - \frac{\ell_0}{\ell(t)}\right]. \tag{25}$$

The solid lines in Fig. 8 are the respective fits with Eq. (25), fixing α to $\frac{1}{3}$. The consistency of all the data sets with the solid lines justifies the method of analysis. In addition, these fittings provide estimates for ℓ_0, from where the scaling regimes start. Of course, in the fitting processes one can treat α as an adjustable parameter. Such an exercise yields essentially the LS value, within $\pm 3\%$ deviation. The results from the fitting exercises are quoted in Table I. There, the (reasonably) systematic variation in ℓ_0 with q may have its origin in the generation of initial configurations via random numbers. In such random initial configurations one expects the average cluster sizes to be smaller for higher q. This fact also plays a role in the late onset of instability or scaling regime for large q.

For an unambiguous estimate of the growth exponent, using finite system sizes ($L \leqslant 256$), we use the FSS analysis, which, in addition, also provides quantitative information on the finite-size effects. As already mentioned in Sec. II B, for performing the FSS analyses we use the saturation domain length $\ell_{\max}$, instead of L. In Figs. 9(a) and 9(b) we show representative plots from the FSS exercise, for which we used the data sets shown in Figs. 6(a) and 6(b). Given that we already have accurate knowledge of ℓ_0, while doing the FSS

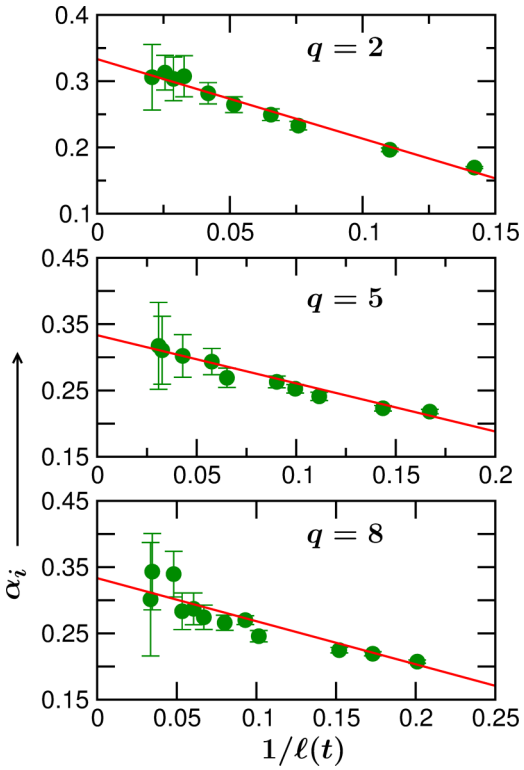

FIG. 8. Plots for the instantaneous exponent α_i versus $1/\ell(t)$, for different q, computed from the data in Fig. 7. The solid lines are fits to the form in Eq. (25), with $\alpha = \frac{1}{3}$. The data in the finite-size affected region have been carefully removed. The error bars represent standard errors of the mean, obtained by averaging over 100 initial realizations.

analysis we tune only the value of α, to obtain the optimum collapse of data. Note that for this analysis we use Eq. (18), which is slightly different from Eq. (7), given that the former contains a subtraction of the time t_0 from t. Since t_0 is the time when $\ell(t) = \ell_0$, the value of the former can be obtained from ℓ_0 by taking the latter from Table I. In this exercise, since we use α as a free parameter, we choose ℓ_0 from the third column in Table I. The values of the corresponding t_0, for $q = 2$ and 6, are quoted in Figs. 9(a) and 9(b).

While reasonable collapse of data, along with the appropriate limiting behavior of $Y(y)$, is obtained for $\alpha = 0.33$ when $q = 2$, for $q = 6$ we obtain it for $\alpha = 0.32$ (consistent with the results in Table I). The solid lines in Figs. 9(a) and 9(b) show consistency of the scaled data sets with the behavior in Eq. (22), in the finite-size unaffected regime. The flat nature of the data in the small abscissa regions is due to the finite-size effects that restrict the growth of the domains. The crossover between these two limiting behaviors appears reasonably sharp, and from the point of deviation from the $y^{-\alpha}$

TABLE I. Results from fittings of Eq. (25) to α_i vs $1/\ell(t)$ data, for different values of q, presented in Fig. 8. We have quoted numbers for ℓ_0 obtained by using α as a fit parameter as well as by fixing α to $\frac{1}{3}$. The reduced (standard) chi-squared χ_r^2 (χ^2/ number of degrees of freedom) measures the goodness of a fit.

q	α	ℓ_0	χ_r^2	ℓ_0 ($\alpha = \frac{1}{3}$)	χ_r^2 ($\alpha = \frac{1}{3}$)
2	0.33(1)	3.67(10)	0.2	3.74(3)	0.2
3	0.33(1)	2.65(20)	0.8	2.75(5)	0.7
4	0.32(1)	2.10(20)	0.6	2.31(5)	0.3
5	0.32(1)	2.17(11)	0.2	2.35(3)	0.3
6	0.32(2)	2.13(15)	0.6	2.10(10)	0.7
8	0.33(3)	2.19(9)	0.9	2.31(13)	0.7
10	0.32(2)	2.08(28)	0.7	2.38(8)	0.8

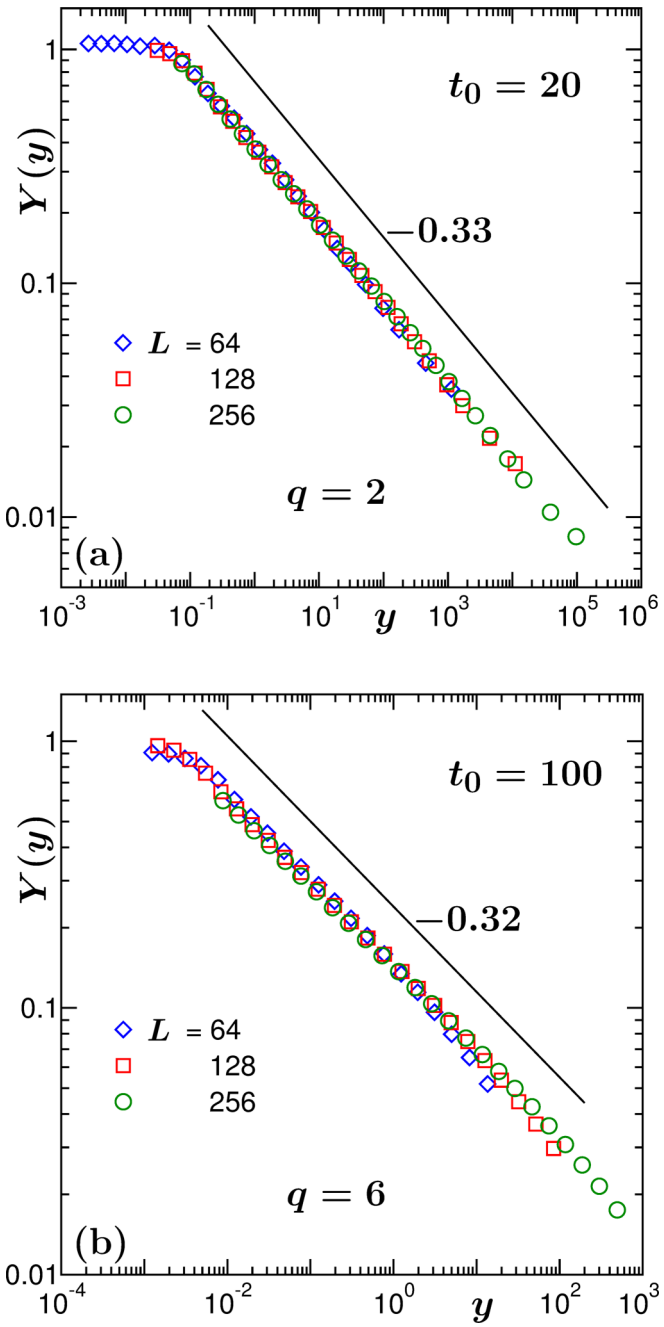

FIG. 9. Finite-size scaling plots, obtained by using data from three different system sizes, for (a) $q = 2$ and (b) $q = 6$, at $T = 0.7\,T_c$. The values of α, related to the optimum collapse of data, are quoted in the respective plots. The solid lines there correspond to the $Y \sim y^{-\alpha}$ behavior of the master curve in the finite-size unaffected regime.

behavior one can obtain an estimate of the onset of finite-size effects [13,14]. For both $q = 2$ and 6, we find that the finite-size effects start when $\ell(t) \simeq 0.8\ell_{\max}$. This is consistent with previous estimates for (solid) binary mixtures [13,14], as well as for fluid phase separation with percolating morphology [30], and suggests that finite-size effects are rather weak. From the consistency of the data (in Fig. 9) with the expected power-law behavior [see Eq. (22)] ($\alpha \simeq \frac{1}{3}$) for $y \gg 0$, it is quite evident that the LS regime is realized rather early.

C. Universal finite-size scaling function

From a look at the data for domain growth, for different q, in Fig. 7, it is apparent that the amplitude A decreases with the increase of q. For a similar behavior in the temperature-dependent cluster coarsening during the collapse of a polymer [38,39], this feature related to A was appropriately incorporated in the analysis by introducing nonuniversal metric factors to extract a universal finite-size scaling function. To check for such universal description, here we follow Refs. [38,39] and modify the scaling variable y in the FSS ansatz and rewrite it as

$$y_q = f_q \frac{(\ell_{\max} - \ell_0)^{1/\alpha}}{(t - t_0)}, \tag{26}$$

where the metric factor

$$f_q = \left[\frac{A(q=2)}{A(q)}\right]^{1/\alpha} \tag{27}$$

takes care of the q-dependent amplitude $A(q)$. Given that by construction $Y = 1$ in the $t \to \infty$ limit, in absence of f_q the scaling functions for different q will be shifted from each other only along the abscissa. Introduction of f_q gets rid of such shifts, for which we treat the $q = 2$ case as a reference. In this scaling exercise (see Fig. 10), we use data from several values of q, quoted inside the frame, along with the values of f_q. The values of f_q were obtained from an optimum collapse exercise with lateral shifts, by fixing α to a reasonable value. Later, we have checked the authenticity of the numbers for f_q by fitting the data sets for growth to the power-law form that contains ℓ_0. We obtain equally good collapse for $\alpha \in [0.31, 0.33]$. In Fig. 10 we show a representative scaling plot for $\alpha = \frac{1}{3}$. An idea about the dependence of f_q on q can be obtained from the table inside the figure. High quality scaling here confirms that the growth behavior, irrespective of the value of q, in finite systems, can be described by a universal scaling function. Such universal feature was previously observed in the context of equilibrium critical phenomena in different models or lattices [50,51].

Next, we briefly discuss the equivalence between the q-state Potts and the $x_c = 1/q$ Ising models. In Fig. 11 we present a comparison between domain growths in the q-component equiproportion mixture (q-state Potts model) and the corresponding off-critical binary mixture (Ising model) with $x_c = 1/q$. As earlier (recall Figs. 4 and 5), the presented results are from $T = 0.6J/k_B$. We have included data sets for two values of q, viz., $q = 4$ and 10. For both the q values, the data for the multicomponent mixture quite nicely overlap with the corresponding binary mixture, thus confirming the equivalence between the two cases. Interestingly, the mismatch in the morphological properties, though small, that we observed

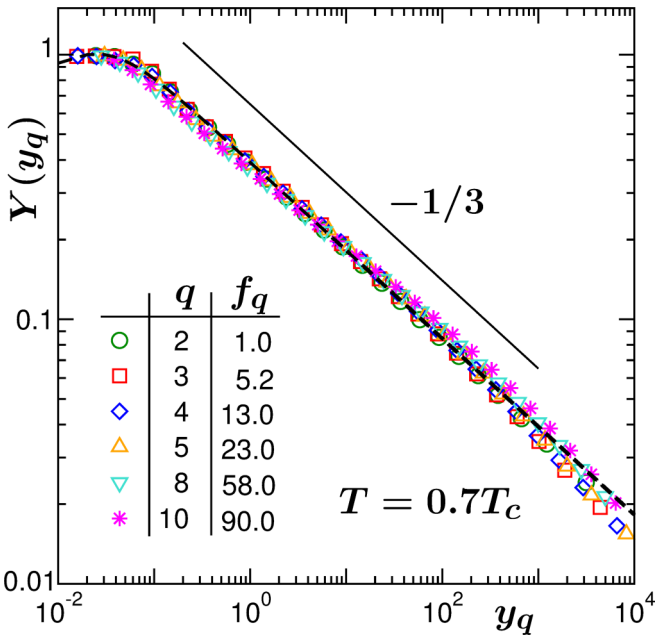

FIG. 10. Demonstration of the fact that the finite-size scaling curves in domain growth for different q can be collapsed onto a single master curve, such that there exists a universal finite-size scaling function $Y(y_q)$, when plotted against the modified scaling variable y_q. The values of the metric factor f_q, used to obtain the optimum collapse of data, are tabulated inside the figure. The results correspond to $L = 128$ and $T = 0.7\,T_c$. The solid line represents the behavior $Y(y_q) \sim y_q^{-\alpha}$, with $\alpha = \frac{1}{3}$. The dashed line represents a fit of Eq. (28) with the ansatz for $f(y_q)$ mentioned in the text.

in $P(\ell_d, t)$ (see Fig. 5), does not get reflected in the domain growth. For the sake of brevity, here we avoid the exercise related to the universal finite-size scaling since a positive outcome is quite obvious. Instead, below we provide a brief discussion on the possible form of the full scaling function $Y(y_q)$.

By observing the limiting forms in Eqs. (16) and (17), and noting from Fig. 10 that $\tilde{X}_0 = 1$, it is meaningful to write

$$Y(y_q) = \frac{1}{p_1 y_q^{\alpha} + \frac{1}{1+p_2 f(y_q)}}, \tag{28}$$

with the requirement that $f(y_q) \to 0$ for $y_q \to 0$ and $[1 + p_2 f(y_q)]$ does not vanish. In an earlier work [14], we used a power-law ansatz for $f(y_q)$ to fit the simulation data for $Y(y_q)$. In that work, the construction of FSS was done in a slightly different way. There, the finite-size unaffected behavior of $Y(y_q)$ was expected to be a constant. This implies the current scaling function matches with that of the previous one when multiplied by $y_q^{-\alpha}$, in addition to the fact that y_q in this work relates to the earlier when it is raised by the power α. The exponent θ of the power-law form $f(y_q) \sim y_q^{\theta}$ here is equivalent to an exponent $\alpha\beta$ of Ref. [14]. The value $\beta \simeq 4$, that was obtained there, corresponds to a rather fast convergence of Y to the expected behavior in the $y_q \to 0$ limit. In our case also $\beta = 4$, i.e., $\theta = \frac{4}{3}$ while fixing $\alpha = \frac{1}{3}$ provides a reasonably acceptable behavior. This is shown by the dashed black line in Fig. 10. The values of p_1 and p_2 are 2.55 and 416, respectively. Similar fitting with $\beta = 2$,

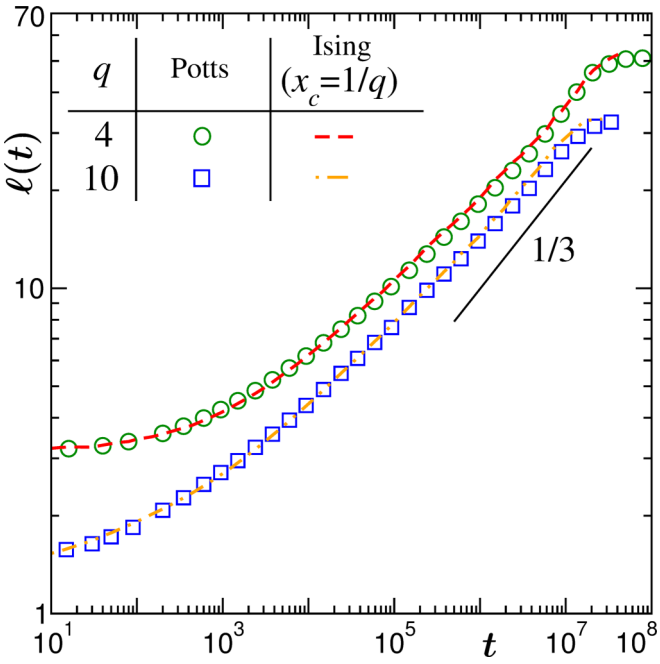

FIG. 11. Comparison of growth of the average domain length $\ell(t)$ between the q-component equiproportion mixture and the off-critical solid binary mixture (with $x_c = 1/q$), for $q = 4$ and 10. All results were obtained from simulations at $T = 0.6J/k_B$, using a system with $L = 128$. The black solid line corresponds to the LS growth. The results are shown on a log-log scale.

however, cannot be ruled out either. In any case, the actual functional form of Y can be trusted only when obtained or justified via appropriate theoretical consideration.

D. Effect of quench temperature

So far, we dealt with a fixed quench depth, viz., $T = 0.7T_c$. In this section we present results from simulations at different T, to check the robustness of the LS growth as well as the universality of the finite-size scaling function.

In Figs. 12(a) and 12(b) we show the growth at three different quench temperatures, for $q = 2$ and 5, respectively. For both the values of q, the data from different quench temperatures, at late time, appear parallel to each other. In the inset of each of the figures we present the corresponding plots for very low temperature, viz., $T = 0.35T_c$. For this temperature, it appears that there is a crossover from an initial slower growth to the LS behavior. In fact, for the Ising model, with equiproportionate (critical) composition, at such low temperature, it has been argued [52–54] that the dominance of interface diffusion over bulk diffusion gives rise to a slower growth with $\alpha = 1/4$. This fact was explained via numerical solution of the Cahn-Hilliard equation with concentration dependent mobility [54] (see also the discussion in Ref. [15]). In the present case, for both the values of q, apparently the data at early time ($t \leqslant 10^4$ for $q = 2$ and $t \leqslant 10^5$ for $q = 5$) are consistent with a growth $\sim t^{0.05}$, shown by the solid lines in the insets of Fig. 12. A fitting of the same data using the form in Eq. (7), however, yields $\alpha \simeq 0.26$ for $q = 2$, consistent with the claim for the Ising model [52–54]. On the other hand, for $q = 5$, the fitting provides a much slower

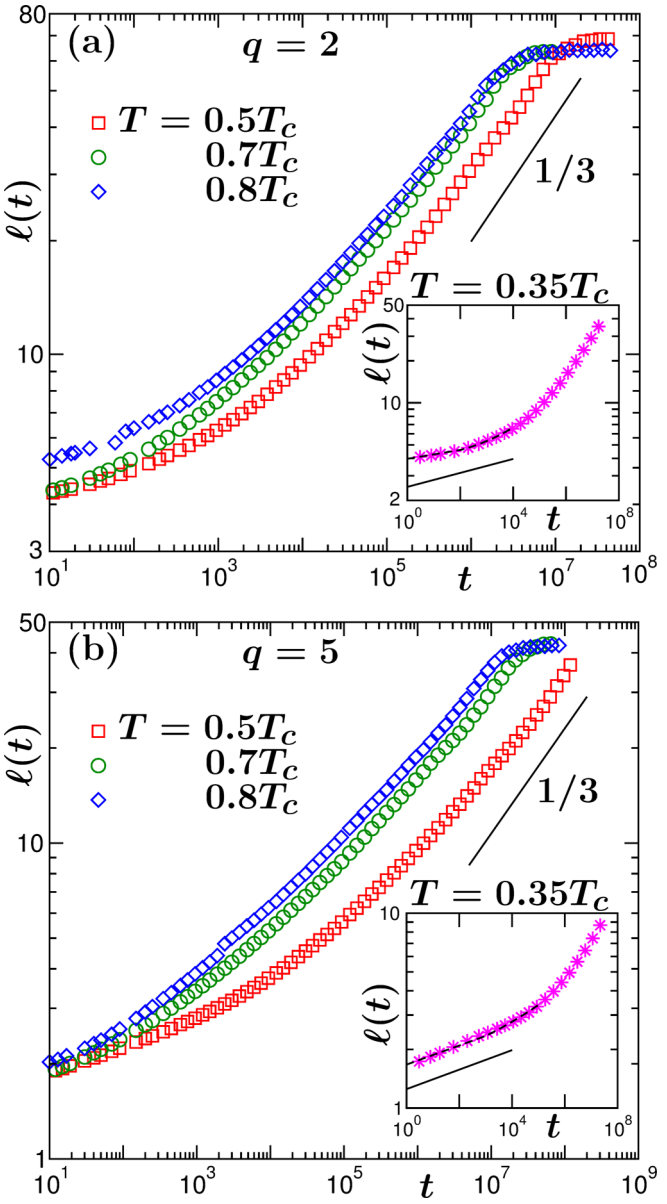

FIG. 12. (a) Double-log plots of the average domain length $\ell(t)$ versus time, for three different quench temperatures, as indicated, for $q = 2$. (b) Same as (a) but for $q = 5$. The solid lines correspond to the LS growth law. The insets in (a) and (b) show the corresponding time dependence of $\ell(t)$ at quite low temperature, viz., $T = 0.35T_c$. There, the dashed lines are obtained from a fit of the early time data ($t \leqslant 10^4$ for $q = 2$ and $t \leqslant 10^5$ for $q = 5$) using the form in Eq. (7) and the solid lines correspond to the power-law behavior $\sim t^{0.05}$.

growth with $\alpha \simeq 0.15$. These fits are shown by the dashed lines in the insets of Fig. 12.

For nonconserved dynamics of the Potts model, for $q > 4$, at low temperatures, it has been argued [55] that the usual scaling of domain growth gets interrupted with a finite probability when the system gets stuck in highly symmetric blocked configurations, viz., striped and honeycomb. For such phases the dynamics is typically guided by the associated characteristic energy barrier [56]. This makes the relaxation of ferromagnetic ordering an order of magnitude slower, i.e., the relaxation time τ diverges as $\tau \sim L^z$ with $2 < z < 4$. For even

lower temperatures, the system may get stuck in disordered metastable states at very early time, giving rise to a glassy behavior [55].

In view of difficulties due to above mentioned reasons, we abstain from further investigation at very low temperatures and shift our focus on the moderate temperature range. As done previously, for obtaining α one could again rely on calculating α_i and fit the form in Eq. (25) to the corresponding data sets. Such exercises, by fixing $\alpha = \frac{1}{3}$, yield ℓ_0 within the ranges [3.5,4.0] and [2.0,2.5], for $q = 2$ and 5, respectively. Realizing the weak temperature dependence of ℓ_0 (notice the narrow ranges), in the subsequent FSS analyses for different quench temperatures, we use the ℓ_0 values presented in Table I.

From the data presented in the main frames of Figs. 12(a) and 12(b), it appears that the growths at different T differ from each other only by constant factors, related to the temperature-dependent amplitude $A(T)$. This could be explained from the temperature dependence of diffusivity, as is well known. Since diffusivity increases with temperature, one expects a faster growth at higher temperatures.

Like in the case of q dependence, here also we construct a similar FSS ansatz just by replacing the scaling variable y_q by

$$y_T = f_T \frac{(\ell_{\max} - \ell_0)^{1/\alpha}}{(t - t_0)}, \tag{29}$$

with a metric factor

$$f_T = \left[\frac{A(T = 0.7\,T_c)}{A(T)}\right]^{1/\alpha}, \tag{30}$$

where we have treated $T = 0.7T_c$ as the reference case. As mentioned above, even though ℓ_0, and correspondingly t_0, slightly vary within the temperature range $0.5 \leqslant T/T_c \leqslant 0.8$, we use constant ℓ_0 and t_0 values, while obtaining the optimum collapse of data for different T. We obtain a reasonable collapse of data with $\alpha \in [0.3, 0.34]$ and [0.29,0.33] for $q = 2$ and 5, respectively, which, within error bars, are again consistent with the LS value. To demonstrate this, in Figs. 13(a) and 13(b) we show representative plots from such exercises with $\alpha = \frac{1}{3}$, for $q = 2$ and 5, respectively. The values of the metric factor f_T used in each case are tabulated inside the figures.

The plots in Fig. 13 show consistency with the expected $Y(y_T) \sim y_T^{-\alpha}$ behavior, in the large y_T regime. Similar exercise for other values of q results in the same universal behavior for $\alpha \in [0.29, 0.34]$. Such observation again confirms the presence of a temperature-independent finite-size scaling of the domain growth for the q-state Potts model, that can be described by a universal finite-size scaling function with a nonuniversal metric factor, dependent only on the amplitude of growth. To this end, we also confirm that the same functional form of Y obtained from fitting Eq. (28) to the data in Fig. 10 fits nicely to the data here, as shown by the dashed lines in both the plots. However, one should be careful that such an analysis is cumbersome for very low temperatures (e.g., for $T = 0.35T_c$) where there is a crossover from an initial slow growth to a faster growth. In such a situation, an appropriate estimation of the (delayed) crossover to the LS scaling regime is needed.

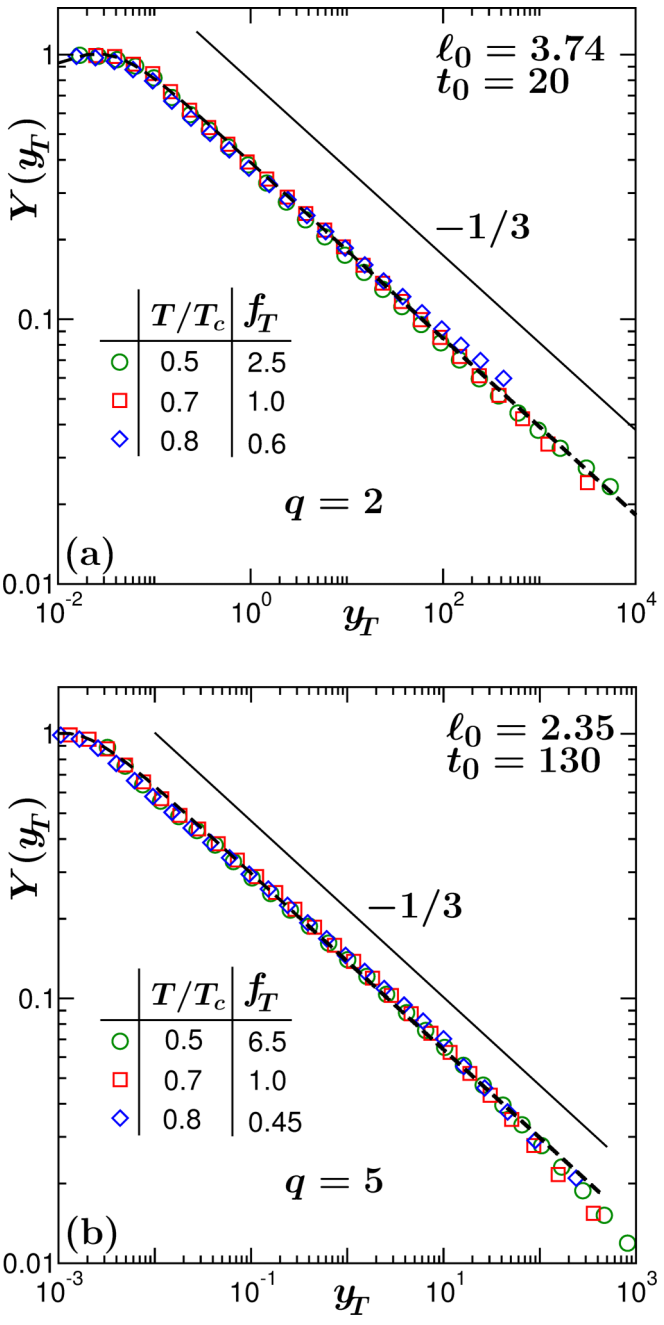

FIG. 13. Plots of the universal finite-size scaling function $Y(y_T)$, versus the scaling variable y_T, using data from different quench temperatures, for (a) $q = 2$ and (b) $q = 5$, with $L = 128$. The values of the metric factor f_T are quoted in the table inside the figures. The solid lines there correspond to the behavior $Y(y_T) \sim y_T^{-\alpha}$, with $\alpha = \frac{1}{3}$. The used values of ℓ_0 and t_0 are also quoted therein. The dashed lines represent the same functional form (28) as plotted in Fig. 10 with its argument y_q being divided by the respective nonuniversal metric factor f_q (= 1 for $q = 2$ and 23 for $q = 5$) mentioned in the table therein.

IV. CONCLUSION

In this paper, we have presented results for the kinetics of phase separation in multicomponent solid mixtures, from

Monte Carlo simulations of the conserved q-state Potts model, in space dimension $d = 2$, for $2 \leqslant q \leqslant 10$. In agreement with a previous report [35], we also find that, even though for a fixed q various morphology-characterizing functions obey the expected scaling relations, there exists no common scaling function for different q. The primary interest in our work was to quantify the domain-growth kinetics. This we achieve via the application of an appropriate finite-size scaling analysis [11–14,30,44]. Like in critical phenomena [44], this technique allows one to obtain a precise estimation of the growth exponent α, without using very large systems. We observe that finite-size effects are weak, as in the Ising model [13,14,30]. By considering an initial domain length [13] in the scaling ansatz, we show that one obtains the Lifshitz-Slyozov growth, for all q, from rather early times, like in the Ising case. This was previously confirmed [35] to be true in the asymptotic limit, via the application of a renormalization-group method of analysis to Monte Carlo results.

More importantly, inspired by recent related results for cluster coarsening during the collapse of a polymer [38,39], we show that the growth for different q can be described by a *universal* finite-size scaling *function*, with a nonuniversal, q-dependent, metric factor, arising from the amplitude of growth (that varies with q). In a similar way, for a range of quench depth, viz., $T \in [0.5T_c, 0.8T_c]$, we show that the growth follows the Lifshitz-Slyozov law, irrespective of the quench temperature, for all q. This also can be described by the same universal finite-size scaling function. Indeed, data for all different q and different quench temperatures that are presented here can be described by the same function obtained from the ansatz in Eq. (28). In view of that, as a concluding plot, we show this behavior in Fig. 14. For this we have modified the scaling variable y to $y_s = f_q f_T (\ell_{\max} - \ell_0)^{1/\alpha}/(t - t_0)$ by taking f_q and f_T from the tables in Figs. 10 and 13. The nice collapse of all the data along with the functional form obtained from the ansatz in Eq. (28) perhaps indicates that the scaling is superuniversal.

Furthermore, our data for moderate systems sizes show that finite-size effects are rather negligible, i.e., they start showing only when the domain length is comparable to the maximum length it can attain, that is, when $\ell(t) \approx 0.8\ell_{\max}$. This result in combination with the findings of a previous work [30] that contains data on the kinetics of liquid-liquid and vapor-liquid transitions, implies that universality with respect to finite-size effects is rather robust in coarsening phenomena with conserved order parameter.

In addition, we have also shown the equivalence between the evolution of a critical (equiproportion) q-component mixture and an off-critical binary mixture with composition of the minority species $x_c = 1/q$. One may ask the following question: What will be the outcome with respect to domain-growth and finite-size effects for off-critical compositions in the q-state Potts model? In such a situation, the mixture may fall in the nucleation and growth regime. In that case, the onset of coarsening will get delayed. As a side remark, we suspect that both thermodynamic and kinetic aspects in this regime, for this model, may have richer features than in the Ising case. Nevertheless, we do not expect any deviation of the growth law from the $\alpha = \frac{1}{3}$ behavior, in the late time regime, for thermodynamically large systems. However, the extraction of the finite-size effects may require certain adjustment. For an equiproportion q-component mixture, the final lengths for all the components are the same. On the other hand, for off-critical compositions, these lengths will differ from each other, being smaller for a component with lower concentration. In this case, one should choose the final length appropriately to obtain a correct understanding of the finite-system-size features. If one considers the growth of the minority species as the reference, including its finite-size limited value, the same universal conclusion on the finite-size effects can be obtained. Recall that this is what was adopted in the case of the Ising model with off-critical composition.

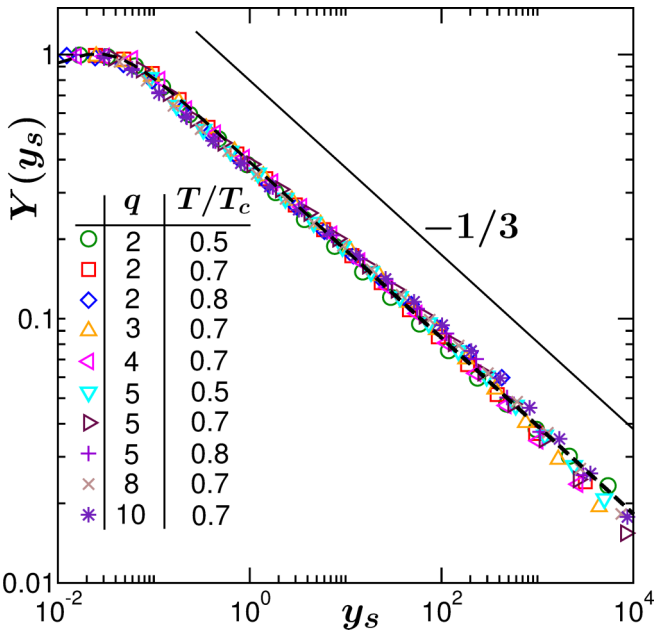

FIG. 14. Plot demonstrating the superuniversal behavior of the finite-size scaling function $Y(y_s)$ versus the scaling variable $y_s = f_q f_T (\ell_{\max} - \ell_0)^{1/\alpha}/(t - t_0)$, obtained by using data for different q and different quench temperatures T. The dashed line corresponds to the functional form obtained using Eq. (28) and the solid line represents the $Y(y_s) \sim y_s^{-\alpha}$ behavior.

Our observations point to the fact that the curvature dependent correction to the growth exponent, that was proposed earlier, is rather weak. This is possibly a consequence of the fact that the leading-order correction to the interfacial tension for Ising-type symmetric models is quadratic in the inverse droplet radius [57–59]. Note that the leading correction proportional to $1/\ell(t)^3$, in Eq. (6), can be obtained by assuming a nonzero Tolman length [60] (prefactor of the above mentioned linear term) in the curvature dependence of the interface tension. However, it has been convincingly shown that the Tolman length is absent in Ising-type systems, at least in space dimension three [57–59].

Another important aspect of phase separation kinetics is the presence of aging and related dynamical scaling [3,61]. It would definitely be interesting to see whether such a universal finite-size scaling function that we discovered for the domain growth exists for this property as well.

ACKNOWLEDGMENTS

The work was funded by the Deutsche Forschungsgemeinschaft (DFG) under Grant No. JA 483/33-1 and further supported by the Deutsch-Französische Hochschule (DFH-UFA) through the Doctoral College "$\mathbb{L}^4$" under Grant No. CDFA-02-07 and the European Union through the FP7 Marie Curie IRSES network DIONICOS under Contract No. PIRSES-GA-2013-612707.

[1] K. Binder, in *Phase Transformation of Materials*, edited by R. W. Cahn, P. Haasen, and E. J. Kramer (Wiley VCH, Weinheim, 1991), Vol. 5, p. 405.
[2] A. J. Bray, Adv. Phys. **51**, 481 (2002).
[3] *Kinetics of Phase Transitions*, edited by S. Puri and V. Wadhawan (CRC Press, Boca Raton, FL, 2009).
[4] M. Rao, M. H. Karlo, J. L. Lebowitz, and J. Marro, Phys. Rev. B **13**, 4328 (1976).
[5] G. S. Grest and P. S. Sahni, Phys. Rev. B **30**, 226 (1984).
[6] D. A. Huse, Phys. Rev. B **34**, 7845 (1986).
[7] C. Roland and M. Grant, Phys. Rev. Lett. **60**, 2657 (1988).
[8] C. Roland and M. Grant, Phys. Rev. B **39**, 11971 (1989).
[9] J. G. Amar, F. E. Sullivan, and R. D. Mountain, Phys. Rev. B **37**, 196 (1988).
[10] J. F. Marko and G. T. Barkema, Phys. Rev. E **52**, 2522 (1995).
[11] D. W. Heermann, L. Yixue, and K. Binder, Physica A (Amsterdam) **230**, 132 (1996).
[12] J. Viñals and D. Jasnow, Phys. Rev. B **37**, 9582 (1988).
[13] S. Majumder and S. K. Das, Phys. Rev. E **81**, 050102(R) (2010).
[14] S. Majumder and S. K. Das, Phys. Rev. E **84**, 021110 (2011).
[15] S. Majumder and S. K. Das, Phys. Chem. Chem. Phys. **15**, 13209 (2013).
[16] D. P. Landau and K. Binder, *A Guide to Monte Carlo Simulations in Statistical Physics* (Cambridge University Press, Cambridge, 2009).
[17] I. M. Lifshitz and V. V. Slyozov, J. Phys. Chem. Solids **19**, 35 (1961).
[18] E. D. Siggia, Phys. Rev. A **20**, 595 (1979).
[19] H. Furukawa, Phys. Rev. A **31**, 1103 (1985).
[20] H. Furukawa, Phys. Rev. A **36**, 2288 (1987).
[21] V. M. Kendon, M. Cates, I. Pagonabarraga, and J.-C. Desplat, J. Fluid. Mech. **440**, 147 (2001).
[22] S. Ahmad, S. K. Das, and S. Puri, Phys. Rev. E **82**, 040107 (2010).
[23] S. Majumder and S. K. Das, Europhys. Lett. **95**, 46002 (2011).
[24] S. Ahmad, S. K. Das, and S. Puri, Phys. Rev. E **85**, 031140 (2012).
[25] K. Binder and D. Stauffer, Phys. Rev. Lett. **33**, 1006 (1974).
[26] H. Tanaka, J. Chem. Phys. **105**, 10099 (1996).
[27] H. Tanaka, J. Chem. Phys. **107**, 3734 (1997).
[28] S. Roy and S. K. Das, Soft Matter **9**, 4178 (2013).
[29] J. Midya and S. K. Das, Phys. Rev. Lett. **118**, 165701 (2017).
[30] S. K. Das, S. Roy, S. Majumder, and S. Ahmad, Europhys. Lett. **97**, 66006 (2012).
[31] S. K. Das, M. E. Fisher, J. V. Sengers, J. Horbach, and K. Binder, Phys. Rev. Lett. **97**, 025702 (2006).
[32] C. Jeppesen and O. G. Mouritsen, Phys. Rev. B **47**, 14724 (1993).
[33] K. Tafa, S. Puri, and D. Kumar, Phys. Rev. E **63**, 046115 (2001).
[34] K. Tafa, S. Puri, and D. Kumar, Phys. Rev. E **64**, 056139 (2001).
[35] S. K. Das and S. Puri, Phys. Rev. E **65**, 026141 (2002).
[36] F. Y. Wu, Rev. Mod. Phys. **54**, 235 (1982).
[37] S. Majumder and W. Janke, Europhys. Lett. **110**, 58001 (2015).
[38] S. Majumder, J. Zierenberg, and W. Janke, Soft Matter **13**, 1276 (2017).
[39] H. Christiansen, S. Majumder, and W. Janke, J. Chem. Phys. **147**, 094902 (2017).
[40] C. Sire and S. N. Majumdar, Phys. Rev. Lett. **74**, 4321 (1995).
[41] C. Sire and S. N. Majumdar, Phys. Rev. E **52**, 244 (1995).
[42] K. Kawasaki, in *Phase Transition and Critical Phenomena*, edited by C. Domb and M. S. Green (Academic Press, New York, 1972), Vol. 2, p. 443.
[43] W. Janke, in *Order, Disorder and Criticality: Advanced Problems of Phase Transition Theory*, edited by Y. Holovatch (World Scientific, Singapore, 2012), Vol. 3, p. 93.
[44] M. E. Fisher, in *Critical Phenomena*, Proceedings of the 51st Enrico Fermi Summer School, Varenna, Italy, edited by M. S. Green (Academic Press, London, 1971), p. 1.
[45] M. E. Fisher and M. N. Barber, Phys. Rev. Lett. **28**, 1516 (1972).
[46] *Finite Size Scaling and the Numerical Simulations of Statistical Systems*, edited by V. Privman (World Scientific, Singapore, 1990).
[47] G. Porod, in *Small-Angle X-Ray Scattering*, edited by O. Glatter and O. Kratky (Academic Press, London, 1982), p. 17.
[48] C. Yeung, Phys. Rev. Lett. **61**, 1135 (1988).
[49] S. Paul and S. K. Das, Phys. Rev. E **96**, 012105 (2017).
[50] V. Privman and M. E. Fisher, Phys. Rev. B **30**, 322 (1984), and references therein.
[51] C.-K. Hu, C.-Y. Lin, and J.-A. Chen, Phys. Rev. Lett. **75**, 193 (1995), and references therein.
[52] H. Furukawa, Adv. Phys. **34**, 703 (1985).
[53] S. Puri, A. J. Bray, and J. L. Lebowitz, Phys. Rev. E **56**, 758 (1997).
[54] S. van Gemmert, G. T. Barkema, and S. Puri, Phys. Rev. E **72**, 046131 (2005).
[55] E. E. Ferrero and S. A. Cannas, Phys. Rev. E **76**, 031108 (2007).
[56] I. M. Lifshitz, J. Exptl. Theoret. Phys. (USSR) **42**, 1354 (1962) [Sov. Phys.–JETP **15**, 939 (1962)].
[57] M. P. A. Fisher and M. Wortis, Phys. Rev. B **29**, 6252 (1984).
[58] B. J. Block, S. K. Das, M. Oettel, P. Virnau, and K. Binder, J. Chem. Phys. **133**, 154702 (2010).
[59] S. K. Das and K. Binder, Phys. Rev. Lett. **107**, 235702 (2011).
[60] R. C. Tolman, J. Chem. Phys. **17**, 333 (1949).
[61] M. Henkel and M. Pleimling, *Non-Equilibrium Phase Transitions, Vol. 2: Ageing and Dynamical Scaling far from Equilibrium* (Springer, Heidelberg, 2010).